ELSEVIER

Physica E 13 (2002) 719–722

PHYSICA E

www.elsevier.com/locate/physe

Magnetotransport through AFM-defined antidot arrays

A. Dorn[a,*], M. Sigrist[a], A. Fuhrer[a], T. Ihn[a], T. Heinzel[a], K. Ensslin[a], W. Wegscheider[b], M. Bichler[c]

[a] *Solid State Physics Laboratory, ETH Zürich, 8093 Zürich, Switzerland*
[b] *Angewandte und Experimentelle Physik, Universität Regensburg, 93040 Regensburg, Germany*
[c] *Walter Schottky Institut, TU München, 85748 Garching, Germany*

Abstract

Finite antidot arrays were fabricated by atomic force lithography using local anodic oxidation. Low-temperature magnetoresistance measurements on a square 20×20 antidot lattice with a period of $a = 300$ nm showed clear commensurability peaks as well as a quenching of the Hall effect around zero magnetic field. In addition B-periodic oscillations were found superimposed on the main commensurability peak around one antidot at temperatures as high as 1.7 K. These observations indicate the high electronic quality of AFM-defined antidot lattices. © 2002 Elsevier Science B.V. All rights reserved.

Keywords: Antidot lattice; Commensurability peaks; AFM-lithography

Magnetotransport experiments on antidot lattices in two-dimensional electron gases (2DEGs) have been of considerable interest over the last 10 years (for a review see [1]). More recent studies on arrays with smaller lattice constants have reported Aharanov–Bohm-type oscillations and indications of a Hofstadter-type bandsplitting [2,3]. Samples are usually fabricated from GaAs–AlGaAs heterostructures containing high-mobility 2DEGs close to the surface. In most traditional approaches, the antidot pattern is first transferred to a PMMA resist layer on the sample surface by means of e-beam lithography. The actual potential modulation is then introduced by etching [4], ion irradiation [5] or by evaporating a top gate onto the developed resist layer [3]. In these cases, the feature size is limited by the proximity effect due to electron backscattering from the GaAs.

Lithography based on scanning probe microscopes (SPMs) is not subject to this limitation and, at least in principle, patterning right down to the atomic scale is possible. Examples for SPM nanostructuring include scratching into a resist layer [6], or directly scratching into the surface of an InAs heterostructure [7], material deposition from the tip onto the substrate [8], or arranging single atoms with an SPM tip [9].

Our approach is to use an AFM with a conducting tip (boron doped Si or TiN) as a tool for local anodic oxidation [10]. If the AFM tip acts as a cathode while the chip that is to be nanostructured is grounded, very local oxidation processes can be performed. A thin water film that naturally forms on the sample surface under ambient conditions serves as the electrolyte. A 2DEG in an AlGaAs heterostructure < 50 nm below the surface is depleted below the oxide lines. This procedure has the advantage, that no further treatment or processing of the surface is needed. Electronically functional quantum wires [11] and quantum dots [12] have been fabricated in this way. The very smooth as

* Corresponding author. Tel.: +41-1-633-2314; fax: +41-1-1146.
E-mail address: dorn@solid.phys.ethz.ch (A. Dorn).

1386-9477/02/$ - see front matter © 2002 Elsevier Science B.V. All rights reserved.
PII: S1386-9477(02)00267-9

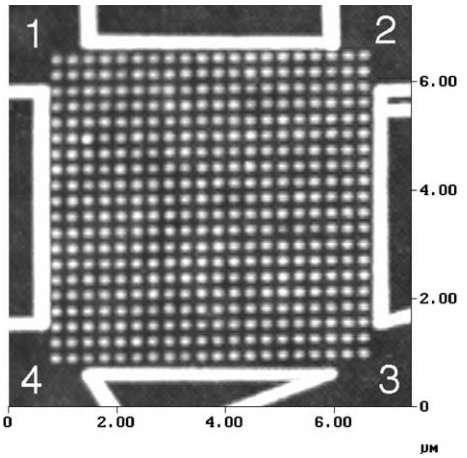

Fig. 1. AFM micrograph of the antidot array and the enclosing cavity. The corners (1–4) served as current and voltage leads.

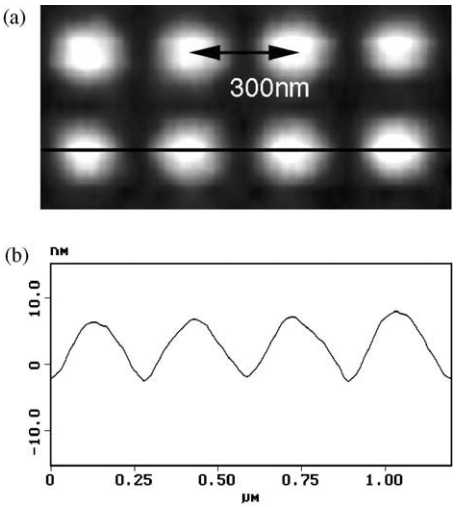

Fig. 2. (a) Closeup of the array in Fig. 1. (b) shows a linescan along the direction indicated above.

well as steep potential walls induced by this method seem ideally suited for the realization of lateral superlattices [10].

Our samples were fabricated from a high quality $GaAs/Al_xGa_{1-x}As$ heterostructure containing a 2DEG 34 nm below the surface with a 4 K mobility of $\mu = 900\,000\ cm^2/Vs$ and an electron density of $N_s = 5\times10^{11}\ cm^{-2}$. Lithography was performed with a commercial digital instruments metrology AFM. A special feature of this AFM are capacitive sensors that compensate long time drifts and hysteresis of the piezos through a hardware feedback. This enables an absolute positioning of the tip with nanometer precision. During the writing process the humidity inside the AFM-chamber was held at a constant value of about 40%. Typical voltages applied to the tip for the oxidation of GaAs were between -10 and -30 V.

The oxide pillars in this structure were written in tapping mode with a stationary 3 s/ $-$ 18 V pulse at each site. Fig. 1 shows the entire 20×20 array enclosed by a square cavity with current and voltage leads in the corners. The bright areas are oxidized and correspond to depleted regions in the underlying 2DEG. The oxide lines forming the cavity are insulating with breakdown voltages > 1 V. As can be seen in Fig. 2(a) and (b), the oxide pillars display a high uniformity and have a base of about 250 nm and a height of about 8 nm. We estimate the error in position to be $\Delta a/a \approx 1\%$ and the variation in antidot size to be less than 5%. The entire structure was then covered with a gold top gate that allows the electron density to be tuned.

The greatest challenges encountered when writing AFM defined antidot lattices are drift and instabilities in the oxidation process. Piezo drifts can be compensated by the hardware as mentioned above, but thermal drift can only be reduced, by ensuring constant laboratory conditions. The oxidation instabilities are probably due to chemical reactions of the tip and/or inhomogeneities and varying amounts of water on the sample surface. These difficulties can be partially avoided by using tips made of chemically inert materials.

The longitudinal resistance R_{xx} was measured diagonally across the array from contact 2 to 4. For the Hall measurements (R_{xy}) terminals 2 and 4 served as current leads while terminals 1 and 3 were used as voltage probes. The commensurability peaks and Hall structures corresponding to cyclotron orbits around 1 and 4 antidots are displayed in Fig. 3. Theoretically these resistance maxima can be explained by a reduced diffusion due to quasi-pinning of the electrons [13]. Similar features have been widely reported in the literature [4]. At higher magnetic fields the cyclotron orbits become smaller than the antidot spacing and the Shubnikov-de Haas (SdH) and quantum Hall effects typical for plain 2DEGs are recovered. From this condition and from the lithographic dimensions

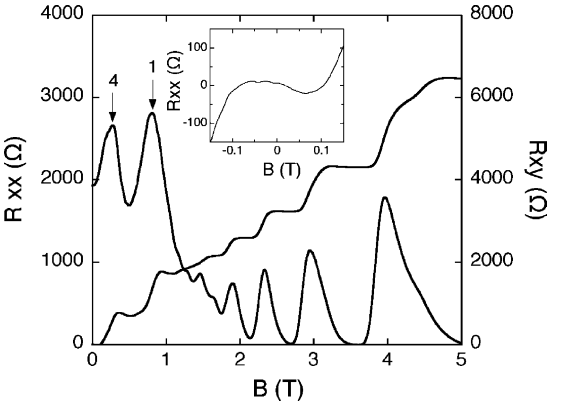

Fig. 3. R_{xx} between leads 2 and 4 and R_{xy} with the current through 2 and 4 and the voltage probes at 1 and 3, at 1.7 K and with a top gate voltage of +100 mV. The inset shows the negative Hall effect around $B = 0$.

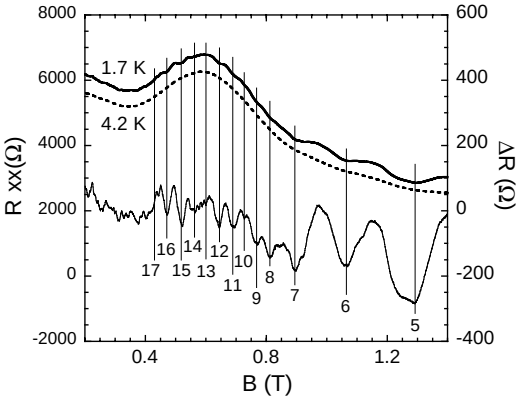

Fig. 4. R_{xx} at 1.7 K (solid line) and at 4.2 K (dashed line, offset by 0.5 KΩ) and the difference between the two (bottom curve). Top gate at −100 mV.

of the oxide dots we estimate the electronic size of the antidots to be smaller than 200 nm. This is consistent with the lateral depletion lengths observed in quantum wires and dots fabricated by the same technology [11,12].

As can be seen in Fig. 4 subtracting an R_{xx} over B trace taken at 4.2 K from a measurement taken at 1.7 K reveals a finer oscillation superimposed on the commensurability peaks. Similar oscillations have been observed in infinite lattices [14] whereas ballistic quantum fluctuations dominate in smaller finite arrays [15]. In our case, the phase coherence length is

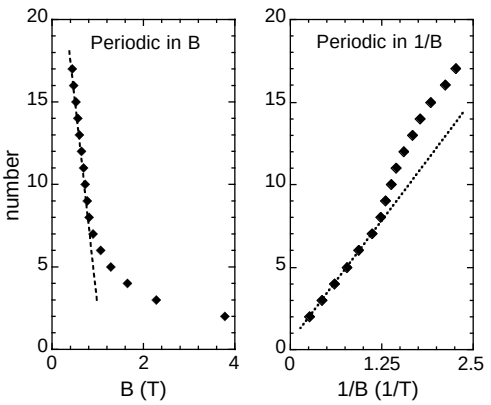

Fig. 5. The minima as determined in Fig. 4 plotted over B and $1/B$. The line fit on the left-hand graph corresponds to a B-periodic oscillation with $B = 41$ mT. The linefit on the right-hand plot follows the positions for SdH oscillations corresponding to an electron sheet density of 2.9×10^{-15} m^{-2}.

larger than the lattice period but probably comparable to or smaller than the enclosing cavity. The observed fluctuations can therefore be expected to be a superposition of both effects.

The oscillations in infinite arrays can be explained in the framework of periodic orbit theory [16]. Stable classical orbits produce a modulation in the quantum mechanical density of states (DOS) that in turn gives rise to resistance oscillations. In addition, the phase matching condition has to be fulfilled. This requires an integer number of flux quanta through the enclosed area. As a consequence, the observed magnetoresistance varies quasi-periodically in B_{flux}. In the simplest case, the periodic orbit encircling one antidot is considered to be dominant. Around this field the Lorenz force is balanced by the electrostatic repulsion from the antidot wall and the cyclotron radius remains approximately constant. Under these conditions the $1/B$ periodicity of the SdH effect is expected to turn into a more B periodic oscillation originating from the effect described above.

Indeed, a transition from $1/B$ to quasi-B periodic behavior was found as can be seen in Fig. 5. The period of about 41 mT corresponds well to the flux quantum through a unit cell of 44 mT or an orbit around one antidot. A number of other smaller peaks also appear. These could be due to phase coherent effects in the cavity or to periodic orbits not considered

in the simplified model. The features described here are similar to the ones found in lattices produced by wet chemical etching [15]. In contrast the modulated top gate technique only induces a weak potential modulation [3] and antidots defined by ion irradiation are less specular [5].

In conclusion, we have demonstrated that high-quality antidot lattices can be fabricated by AFM-lithography. Commensurability peaks and Hall plateaus, the negative Hall effect as well as resistance oscillations from quantized periodic orbits were observed. Future efforts will concentrate on elucidating the exact nature of the induced potential modulation as well as reducing the feature size and improving writing stability.

We are grateful to the Swiss Science Foundation (Schweizerische Nationalfonds) for financial support.

References

[1] R. Schuster, K. Ensslin, Festkörperprobleme 34 (1994) 195.
[2] T. Schlösser, K. Ensslin, J.P. Kotthaus, M. Holland, Europhys. Lett. 33 (1996) 683.
[3] C. Albrecht, J.H. Smet, K. von Klitzing, D. Weiss, V. Umansky, H. Schweizer, Phys. Rev. Lett. 86 (2001) 147.
[4] D. Weiss, M.L. Roukes, A. Menschig, P. Grambow, K.v. Klitzing, G. Weinmann, Phys. Rev. Lett. 66 (1991) 2790.
[5] R. Schuster, K. Ensslin, J.P. Kotthaus, M. Holland, C. Stanley, Phys. Rev. B 47 (1993) 6843.
[6] M. Wendel, H. Lorenz, J.P. Kotthaus, Appl. Phys. Lett. 67 (1995) 3732.
[7] J. Cortes Rosa, M. Wendel, H. Lorenz, J.P. Kotthaus, M. Thomas, H. Kroemer, Appl. Phys. Lett. 73 (1998) 2684.
[8] H.J. Maiman, P.H. Guethner, D. Rugar, Phys. Rev. Lett. 65 (1990) 2418.
[9] D.M. Eigler, E.K. Schweizer, Nature 344 (1990) 524.
[10] T. Heinzel, R. Held, S. Lüscher, K. Ensslin, W. Wegscheider, M. Bichler, Physica E 9 (2001) 84.
[11] R. Held, S. Lüscher, T. Heinzel, K. Ensslin, W. Wegscheider, Appl. Phys. Lett. 75 (1999) 1134.
[12] S. Lüscher, A. Fuhrer, R. Held, T. Heinzel, K. Ensslin, W. Wegscheider, Appl. Phys. Lett. 75 (1999) 2452;
U.F. Keyser, H.W. Schumacher, U. Zeitler, R.J. Haug, K. Eberl, Appl. Phys. Lett. 76 (2000) 457.
[13] R. Fleischmann, T. Geisel, R. Ketzmerick, Phys. Rev. Lett. 68 (1992) 1367.
[14] D. Weiss, K. Richter, A. Menschig, R. Bergmann, H. Schweizer, K.v. Klitzing, G. Weinmann, Phys. Rev. Lett. 70 (1993) 4118.
[15] R. Schuster, K. Ensslin, D. Wharam, S. Kühn, J.P. Kotthaus, G. Böhm, W. Klein, G. Tränkle, G. Weinmann, Phys. Rev. B 49 (1994) 8510.
[16] M.C. Gutzwiller, Chaos in Classical and Quantum Mechanics, Springer, New York, 1990.